Microporous and Mesoporous Materials 125 (2009) 90–96

Contents lists available at ScienceDirect

Microporous and Mesoporous Materials

journal homepage: www.elsevier.com/locate/micromeso

Mechanism of benzene diffusion in MOF-5: A molecular dynamics investigation

Saeed Amirjalayer, Rochus Schmid *

Lehrstuhl für Anorganische Chemie 2, Organometallics and Materials Chemistry, Ruhr-Universität Bochum, Universitätsstr. 150, D-44780 Bochum, Germany

ARTICLE INFO

Article history:
Received 2 December 2008
Received in revised form 29 January 2009
Accepted 2 February 2009
Available online 13 February 2009

Keywords:
Molecular dynamics simulation
Self-diffusion
Metal organic framework
Diffusion mechanism

ABSTRACT

In this contribution, the diffusion of benzene in the porous metal organic framework MOF-5 is investigated by molecular dynamics simulations. Previously, we have shown that by using a first principles derived fully flexible force field the experimentally determined self-diffusion coefficients D_{self} could be well reproduced [S. Amirjalayer, M. Tafipolsky, R. Schmid, Angew. Chem. Int. Ed. 46 (2007) 463]. Here, we use the same methodology to determine the loading dependence on the diffusion. It is found that diffusivity, which is in the range of liquid benzene, slightly increases up to a load of 32 molecules per unit cell and then falls off at higher load. Free energy maps reveal that additional sites appear at higher load due to attractive guest–guest interactions. The topology of these sites is very close to the experimentally determined locations of ferrocene molecules in MOF-5, which corroborates that attractive $\pi-\pi$ interactions govern these systems. The site–site and site-phenylene distances are very similar to the first solvation radius of liquid benzene. For the very open MOF-5, the main barrier for diffusive transport is to overcome the attractive interaction in the binding pockets, which is in contrast to zeolitic microporous systems, where the barrier for diffusion is the hindrance of the pore window. Spatial free energy maps are used to investigate the diffusion pathway on a molecular level and the load dependence of the free energy barriers for these transport processes.

1. Introduction

Porous Coordination Polymers, today mostly referred to as metal organic frameworks (MOFs), have recently gained increasing interest as a potential new class of functional materials [1–3]. Their very large pores and high inner surfaces areas offer a wide range of promising applications in gas storage, separation, sensing and catalysis [4]. Due to their hybrid nature and the modularity of the organic and inorganic building units, a rational design of the functions of the porous material appears to be possible [5]. For all possible applications of such a porous material, the specific nature of the host–guest interactions is of prime importance. Both experimental and theoretical investigations have up to now primarily focused on small, weakly interacting gaseous guest molecules like hydrogen or methane. In particular, the potential of these materials to be used as hydrogen storage has been studied intensively both experimentally and theoretically [6–29]. However, the "thermodynamic" property of gas adsorption (adsorption isotherms) is less sensitive to the peculiarities of the host–guest interaction as compared to the "kinetic" property of self-diffusion. Transport parameters of guest molecules are of similar relevance for a technical use of MOFs in any field. Interestingly, guest molecule diffusivity in MOFs was first studied by means of molecular mechanics (MM) based molecular dynamics (MD) simulations [30,31], using strategies well established for porous zeolitic materials [32,33], before the first measured self-diffusion coefficients were published by Stallmach et al. [34]. In the majority of theoretical investigations on MOFs, a rigid framework was used with the experimentally determined structure, which is mainly due to missing force field parameters for the inorganic parts of the coordination polymer. Recently, a number of parametrizations for MOFs have appeared, which allow to include the full flexibility of the lattice [35–40]. An excellent overview over the current status of theoretical modeling of MOFs can be found in the recent review by Keskin et al. [41].

With the exception of the work by Salles et al. [42] on the framework MIL-53, all these studies (as well as the first self-diffusion measurements [34]) focused on the possibly most investigated MOF-5 ($Zn_4O(BDC)_3$; BDC = benzyldicarboxylate) [43]. In the seminal paper by Eddaoudi et al., the series of isoreticular MOFs (IRMOFs) was introduced, which are derived from the parent structure MOF-5 by variations in the organic linker, demonstrating the possibility to design the pore size [5]. The unit cell of the cubic MOF-5 is shown in Fig. 1. Due to the planarity of the BDC-linkers, the unit cell is formed by two sets of different cubic pores. The slightly larger A-cells are characterized by the planes of the linker's phenylene units facing inwards, whereas in case of the B-cells the phenylene hydrogens point inside the cells. Note, that a

E-mail address: rochus.schmid@rub.de (R. Schmid).
URL: http://aci2.rub.de/schmid (R. Schmid).

1387-1811/$ - see front matter © 2009 Elsevier Inc. All rights reserved.
doi:10.1016/j.micromeso.2009.02.006

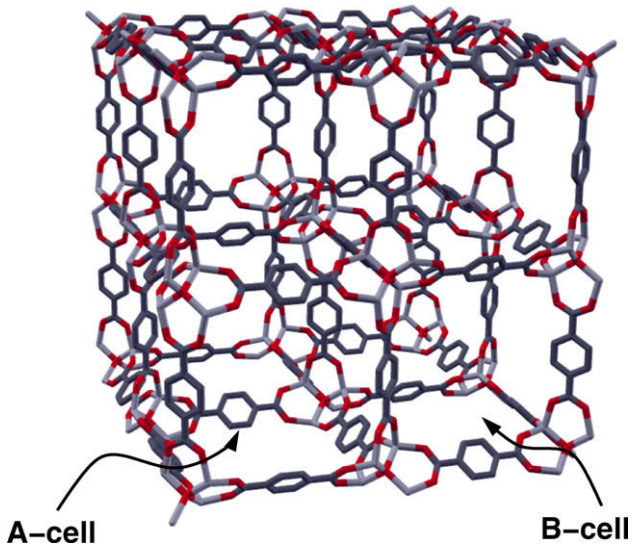

Fig. 1. Structure of the unit cell of MOF-5 showing the two different cubic A- and B-cells.

supramolecular isomer with a non-planar linker (orthogonal carboxylic planes) is possible, where all cells are exactly equal. Using our first principles derived force field [40] we have analyzed this possibility for a number of members in the IRMOF family [44]. For sterically hindered or flexible linkers this isomeric structure becomes more likely, but for MOF-5 the planarity of the linker is strongly preferred.

Our force field is based on reference data calculated by first principles DFT methods for non-periodic model systems. The MM3 force field by Allinger et al. [45–47], which is known to give reliable conformational energies for organic molecules, was extended with a parametrization for the inorganic part (using a bonded model for the Zn–O coordination bonds) in order to reproduce both structure and vibrational modes of the reference calculations. Bond dipoles used in MM3 to represent electrostatic interactions have been derived from DFT calculated atomic charges. As a first test of our new force field we calculated the self-diffusion coefficients of benzene in MOF-5 at experimental loading for different temperatures [48]. The computed value of $D_{self} = 2.4 \times 10^{-9}$ m^2 s^{-1} room temperature matches well with the fastest component ($D_{self} = 2.0 \times 10^{-9}$ m^2 s^{-1}) of the range of diffusivities, found experimentally by using pulsed-field gradient (PFG) NMR techniques [32,49] for this system [34]. It is still not completely clear, whether the origin of the distribution of self-diffusion coefficients in the experimental measurements is due to remaining solvent molecules, defects in the crystals or whether it has other reasons. Our theoretical value has been corroborated independently with another force field by the group of Snurr and coworkers [36]. One important result of this investigation was, however, the observation that more than 90% of the benzene molecules reside in the A-cells in the time average. By an analysis of the spatial probability density of the centers of mass (COM) of the guest molecules, eight distinct binding pockets in the corners of the A-cell were identified. These principle interaction sites have been observed previously. Rowsell et al. investigated the adsorption sites of Ar and N_2 by low temperature single crystal X-ray diffraction [50]. They found similar sites for the accumulation of the guest molecules, but because of their smaller size, a larger number of five sites for Ar and four sites for N_2 were located. These results were confirmed by theoretical investigations by Dubbeldam et al. [25]. Yildirim et al. used neutron diffraction to analyze the adsorption of hydrogen in MOF-5, again corroborating the findings of Rowsell and Dubbeldam [10]. However, they pointed out that at very high loading new adsorption sites for hydrogen are observed, which can be described as the formation of nanocages, built up from the guest molecules.

In this contribution, we have systematically investigated the nature of the host–guest interactions of benzene in MOF-5, using the same theoretical approach as in our previous work [48], focusing on the topology of the binding sites within the pores and the resulting molecular diffusion mechanism. In particular, we investigated how these features and the diffusivities depend on the loading of the system at room temperature. In the next section the computational methods and the simulation setup is presented. In the following section the results are discussed. The final section provides concluding remarks.

2. Computational details

The *TINKER* program package [51] was used to perform the classical molecular mechanics calculations with our extended MM3-force field [40], using a periodically replicated system of the unit cell (uc) containing eight Zn_4O units. A 12.0 Å cutoff for the van der Waals (vdW) interaction and a 10.0 Å cutoff for the electrostatic dipole–dipole interaction were used [52]. The parameters for the organic linker were all taken unmodified from the standard MM3 parameter set [53]. In order to reduce the computational effort, the adjustment of bond stretch and torsion parameters based on the quantum mechanic calculation of π-bond orders by the Pariser–Parr–Pople scheme [54], has been switched off. Instead, the adjusted parameters have been predetermined for a reasonable model system and were kept fixed throughout the simulations. A listing of the full parameter set is given in [40]. The MD simulations were performed by the modified Beeman propagator [55] as implemented in the TINKER package [51], using a timestep of 1.0 fs, which was checked to yield energy conserving microcanonic dynamics. A preliminary lattice optimization of MOF-5 resulted in a lattice parameter of 25.9457 Å. A constant pressure dynamics run (NPT ensemble) of the loaded system showed only small oscillations around this value. Thus, all MD calculations were performed in an NVT ensemble for this fixed lattice parameter. Each of the 10 trajectories were started from a different configuration, generated from a high temperature simulation at 1000 K, in order to avoid any correlations. The final analysis has been performed on the averaged data from all trajectories, whereas statistical errors have been calculated from the standard error of the 10 individual runs. The initial velocities were randomly generated according to a Boltzmann distribution at a given temperature, and a temperature of 300 K was maintained by a Nose-Hoover chain thermostat [56,57]. Note, that the velocity scaling Berendsen thermostat, which is the default in the TINKER code, and which was used by us and others [48,58–60], can lead to deviations in the energy equipartitioning [61]. The first 500 ps were discarded as an equilibration period. From the 3 ns trajectories the last 2.5 ns were used for the analysis, with a configuration stored every 0.1 ps (every 100 timesteps). Thus, per trajectory a total of 25,000 configurations were stored and used for the further analysis. The loading of the unit cell was varied between 10, 20, 32 and 56 benzene molecules. The probability density was generated from the COM trajectories (with the COM positions folded back into the simulation domain) in a 80^3 point mesh and was analyzed and rendered with the program VMD [62]. To improve the statistics of our calculations we used the symmetry of the loaded framework to symmetrize the probability densities. The error estimate for the diffusion coefficients, the free energy barriers and the positions of these barriers are taken as twice the standard error, calculated from the standard deviation from the 10 trajectories, following our previous work

[48]. The room temperature self-diffusion coefficient of liquid benzene was determined in a similar setup as the loaded MOF-5 simulations (118 benzene molecules in a periodic cubic simulation cell of 25.9457 Å size), averaging over five individual trajectories with 0.5 ns equilibration and 1.5 ns sampling time.

3. Results and discussion

3.1. Load dependence of self-diffusion constants

In our previous work, we used a load of 10 benzene (bz) molecules per uc, which is slightly above the load of 6.3 molecules per uc in the experimental work (80 mg/g = 8 wt% [34]). This is low enough to avoid a substantial guest–guest interaction, but sufficient to improve the sampling statistics. The analysis revealed 32 binding pockets in the corners of the A-cells. This binding site coincide with the potential energy minimum of a single benzene molecule inside the pores. Consequently, at a load of 32 bz/uc all of these binding sites would be occupied. In order to study the load dependence we therefore investigated loads of 10, 20, 32 and 56 bz/uc. Note that by assuming a free volume of 80% [5] the density of the benzene phase inside the framework (excluding the volume and weight of the MOF) at a load of 32 bz/uc is 0.23 g/ml, which is about a quarter of the density of liquid benzene (ρ = 0.8765 g/ml [63]).

According to Einstein's equation

$$D_{self} = \frac{1}{6}\lim_{t\to\infty} d/dt\left\langle |\mathbf{r}(t) - \mathbf{r}(0)|^2 \right\rangle, \quad (1)$$

the self-diffusion coefficient D_{self} can be calculated from the slope of the mean square displacements (MSDs) of the benzene's centers of mass (COM), plotted over the time difference (averaged over multiple time origins). Again, following prior work, the self-diffusion was determined by a linear fit in a Δt range of 250–1000 ps, where a diffusive behavior is observed (slope of one in a double logarithmic plot of MSD over Δt for all loads) and on the other hand statistics are good enough. The values of the D_{self}, together with the statistical deviations are given in Table 1. Note, that besides a different thermostat (see Section 2), an identical simulation setup has been used as in our previous investigation. Due to the different starting configurations a somewhat different D_{self} of $2.159 \pm 0.378 \times 10^{-9}$ m^2/s for the load of 10 bz/uc is found, compared to the previous value of 2.49×10^{-9} m^2/s [48], which is, however, within the statistical error. The variation of D_{self} with respect to the load is plotted in Fig. 2. Overall, we observe only modest changes in the diffusivity for different loads. From the averaged values of D_{self} a type IV behavior [64] with an increase at intermediate load and a fall off at high load appears plausible. This type of the load dependence would be consistent with the substantial guest–guest interaction, but due to the larger statistical error bars at lower load a clear-cut conclusion can not be drawn. Such a type IV behavior is observed for strongly interacting guest molecules like benzene also in case of certain zeolites like faujasite Na–Y [33]. Interestingly, all values are very close to the self-diffusion coefficients determined experimentally for liquid benzene, which are in the range of 2×10^{-9} m^2/s to 3×10^{-9} m^2/s [65–68]. Depending on the force field, theoretical investigations of D_{self} of liquid benzene at room temperature found values between 1.4×10^{-9} m^2/s and 4×10^{-9} m^2/s [68–71]. With our MM3 type force field a self-diffusivity of $D_{self} = 1.89 \pm 0.22 \times 10^{-9}$ m^2/s was calculated. In contrast to that, D_{self} for benzene at room temperature in other porous materials like the zeolites Na–X or Na–Y is at least two orders of magnitude smaller [72,73]. This already demonstrates the open structure of MOF-5 and the high mobility of the guest molecules in this material.

Is this true, or does the load dependence change because of the relative amounts of liquid/vapor phase?

Table 1
Self-diffusion coefficient D_{self}, free energy barrier $\Delta G^{\ddagger}$ and position of the free energy barrier $r^{\ddagger}$ for the diffusion process of benzene within MOF-5 (the superscript ‡ refers to the maximum of ΔG).

bz/uc	D_{self} [10^{-9}m^2/s]	$\Delta G^{\ddagger}$ [kJ/mol]	$r^{\ddagger}$ [Å]
10	2.159 ± 0.378	11.51 ± 0.23	15.36 ± 0.19
20	2.628 ± 0.408	10.05 ± 0.13	15.42 ± 0.11
32	2.595 ± 0.203	8.10 ± 0.12	15.40 ± 0.11
56	2.102 ± 0.158	6.27 ± 0.01	12.0 ± 0.01

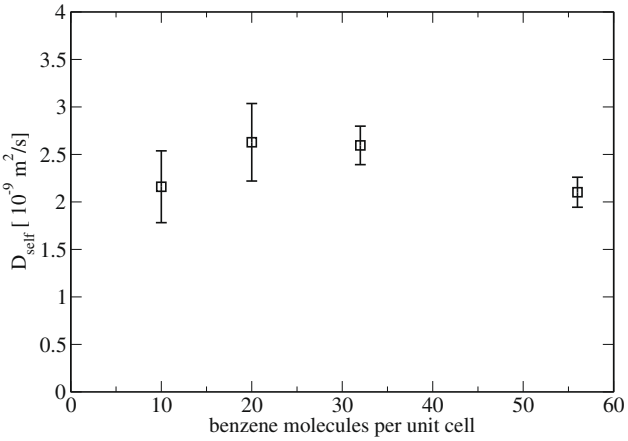

Fig. 2. Dependence of D_{self} of benzene in MOF-5 with respect to the loading.

3.2. Topology of the binding sites

From the spatial probability density $q(\mathbf{r})$ for finding a benzene COM at the point $\mathbf{r}$ (calculated from all trajectories, see Section 2) a spatial free energy map can be derived by

$$\Delta G(\mathbf{r}) = -RTln[q(\mathbf{r})] \quad (2)$$

with the global minimum (highest $q(\mathbf{r})$) taken as the zero of the free energy (with the gas constant R and the temperature T) [74]. In Fig. 3 this free energy map is visualized by isosurfaces for a value of $\Delta G = 5$ kJ/mol. Since $q(\mathbf{r})$ represents the probability of finding the COM of a guest molecule at a given point, irrespective of the orientation of the molecule, the free energy includes the phase space sampling over all 33 internal and rotational degrees of freedom of the benzene molecule (as well as the framework degrees of freedom). Thus, also the entropic contributions (wider phase space) in the inner space of the cell is included in ΔG. In analogy to the maxima of the probability distribution, 32 minima of ΔG in the corners of the A-cells are observed for 10 bz/uc, which are referred to as α_1 sites in the further discussion. This picture does not change significantly by a doubling of the load. However, at 32 bz/uc, a further "site" α_2 appears in the center of the A-cell. At this load, all the primary binding sites α_1 can be populated in principle. Because of the strong $\pi-\pi$ interaction between benzene molecules [75,76] it is now much more likely for one benzene molecule to move into the center of the A-cell, and the free energy is reduced below the threshold of $\Delta G = 5$ kJ/mol. The most apparent change in the free energy map is observed at the highest load of 56 bz/us. Here all the 36 α_1 and α_2 sites can be populated and new free energy minima appear now in the B-cell. These β sites are now, however, not located in the corners but above the faces of the cubic cell. Obviously, the different orientation of the linker phenylene moieties in the B-cell disfavors the corners, whereas the position between four linkers in the face is preferred. The major stabilization of the β site arises from guest–guest interactions with benzene molecules in α_1, since the ΔG at the β site is reduced by more than a factor of two by increasing the load from 10 bz/uc to 56 bz/uc.

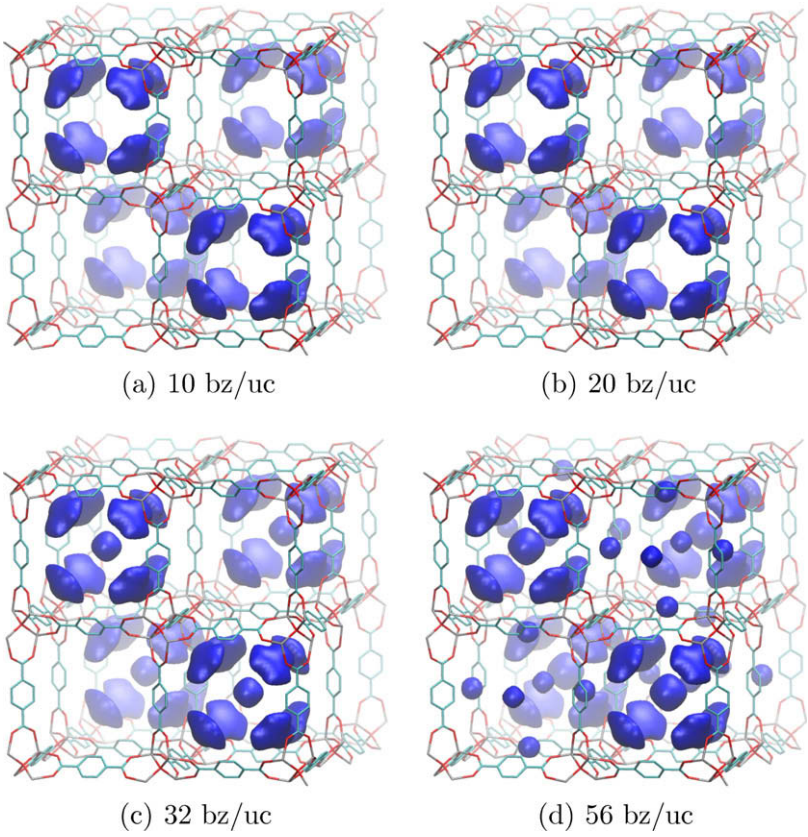

Fig. 3. Free energy map of benzene in MOF-5 for different loadings. Shown is the isosurface for a value of $\Delta G = 5$ kJ/mol.

It is very instructive to compare the distances between these individual sites and the phenylene moiety of the framework with the COM pair correlation functions of liquid benzene at room temperature and standard pressure [77]. The COM position of one phenylene unit in fractional coordinates is with [1/4,0,0] defined by the topology of the network (center of the edge of an A-cell). The same holds with [1/4,1/4,1/4] for the α_2 site, centered in the A-cell. The location of the free energy minima for a selected α_1 and β site with [0.117,0.117,0.117] and [1/4,−0.050,1/4], respectively, was determined from the free energy map for 56 bz/uc (Fig. 3d). From these site positions the following distances can be calculated: The primary α_1 site is surrounded by three phenylene units of the framework with a COM distance of 5.5 Å. This corresponds very well with the values obtain for the first maximum of the pair correlation function of liquid benzene at ambient conditions (ca. 5.5 Å [77], ca. 5.4 Å [78] ca. 5.2 Å [79] for the first shell). In addition to that, the secondary α_2 site is with 6.0 Å distance from α_1 located again at the position of the first solvation shell of liquid benzene with a coordination number of eight, which is somewhat smaller as the value of 13 determined for neat benzene [77]. Note that the α_2 site is formally surrounded by a "second shell" of 12 phenylene units with a distance of 9.2 Å. The distance from the β site to α_1 and the closest phenylene unit is with 6.5 Å and 6.6 Å slightly larger, but still very close to the first solvation radius in liquid benzene. One reason for these observations is the fact that the metric of the cubic MOF-5 framework corresponds well to the first solvation radius of about 5.5 Å of benzene. Because of the cell parameter d = 25.95 Å the diagonal of a cubic cell is $\sqrt{3}\frac{d}{2} = 22.47$ Å, which is four times 5.62 Å. Of course, there is an additional interaction of the guest molecules with the inorganic nodes, leading to the high stabilization of the primary α_1 site. However, the above analysis clearly shows that MOFs can be considered as some kind of "solid solvent".

Apart from the similarity between the COM distances of the aromatic systems (benzene and phenylene units) with the first maximum of the COM pair distribution function of liquid benzene, there is another indirect confirmation for the topology of the binding sites, observed in our simulations. Recently, Kim et al. were able to solve the crystal structure from the synchrotron X-ray diffraction analysis of a MOF-5 single crystal [80], fully loaded with ferrocene molecules by vapor phase impregnation [81]. The ferrocene guest molecules interact so strongly with each other and the matrix that a crystalline long range order is observed and the positions of the guest molecules could be determined with only modest disorder. In Fig. 4, this structure for just one A- and B-cell is shown with the disorder removed for clarity. Clearly, in the A-cell eight guest molecules are found in the corners of the cubic cell, whereas in the B-cell another six ferrocene molecules are located above the faces of the cube. Thus, the topology is identical to the one found in the simulations for a high load of benzene, apart from the α_2 site. Due to the size of the ferrocene molecules, there is not enough space in the center of the A-cell for another guest molecule.

3.3. Benzene diffusion mechanism

From the topology of the free energy maps for the different load, the molecular diffusion mechanism can be derived. Already in our previous study we found that at low load the diffusion proceeds by a jump from one A- to the next A-cell by diagonally moving through the B-cell [48]. The question now is, whether the additional free energy minima at higher load change this picture and how. In order to clarify this, the probability density for the lower half of the unit cell (two A- and two B-cells) were integrated up along the z-coordinate, and by Eq. (2) a 2D free energy map in the xy-plane was calculated. Contour plots are shown in Fig. 5 with isoline separations of 1 kJ/mol. Note that these 2D maps are not

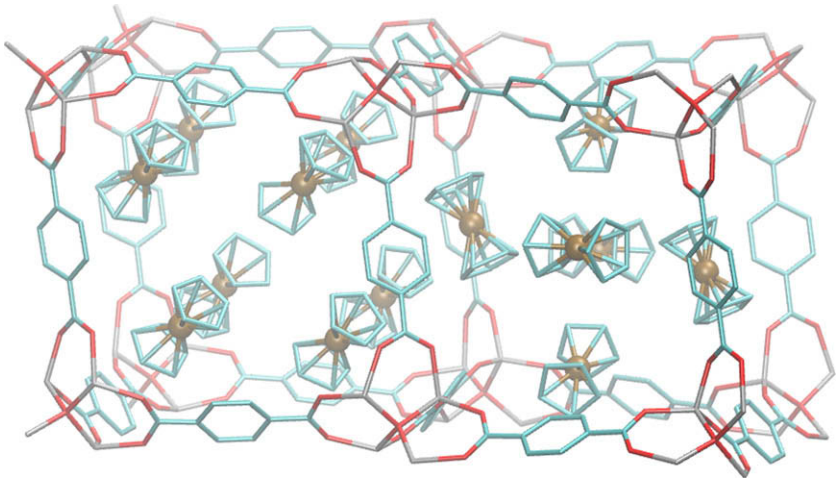

Fig. 4. Single crystal structure of MOF-5 fully loaded with ferrocene molecules from [80]. The disorder of the cyclopentadienyl rings has been removed for clarity.

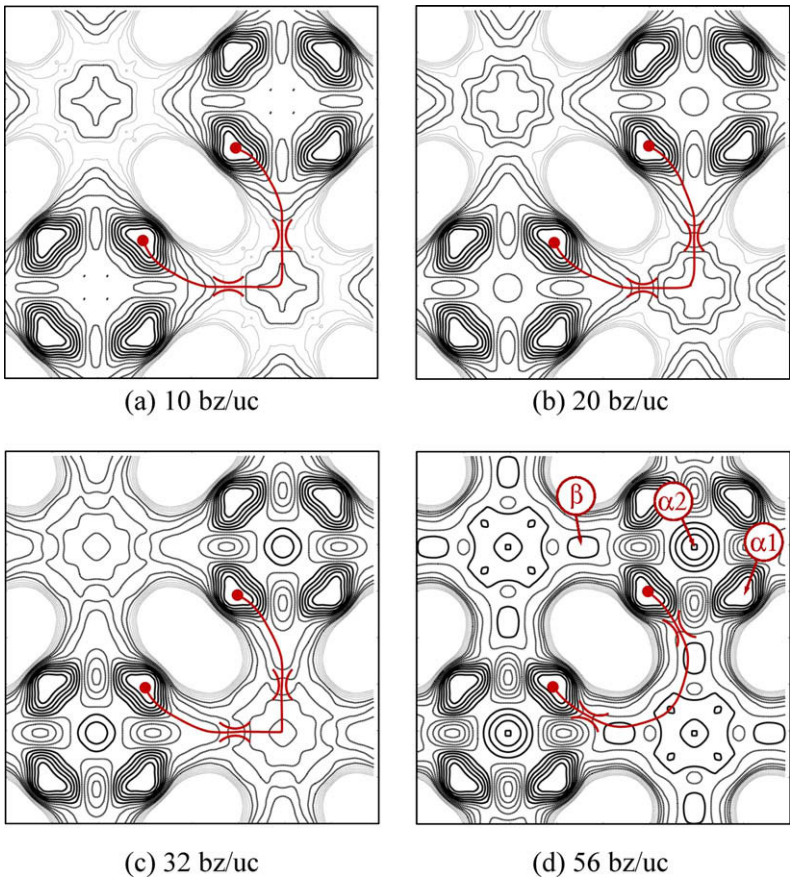

Fig. 5. 2D free energy maps for benzene in MOF-5 at different loading. The contour plots show the ΔG relative to the eight minima in the A-cells (bottom-left and top-right) with a spacing of the isolines of 1 kJ/mol. Thick dark lines: 1–5 kJ/mol; thinner black lines: 6–10 kJ/mol; light grey lines: 11–15 kJ/mol. The 2D diffusion path with the position of the free energy maximum is indicated by a line connecting the A-cell minima. The locations of the α_1, α_2 and the β site are designated in (d).

slices of the 3D map. Because of the z-integration, each of the minima in the A-cell (bottom-left and top-right in Fig. 5) corresponds to two spatial sites seen in Fig. 3. Thus, the $\Delta G(x, y)$ value in this graph gives the free energy with respect to the α_1 site global minima for a guest molecule with its COM constrained to this particular x- and y-coordinate, sampling all other $3N-2$ degrees of freedom. Again, for 10 and 20 bz/us the picture looks very similar. There is no free energy minimum in the center of the A-cell. There is, however, a local free energy minimum around 10 kJ/mol in the center of the B-cell. Thus, in order to move from an α_1 site in one A-cell to another in the adjacent A-cell, the guest molecules have to follow a path indicated in Fig. 5 through the B-cell. The free energy barrier is located at the "window" between A- and B-cell. For a load of 32 bz/uc the whole free energy surface is more flat and the local minima in the center of the A-cells become visible. However, both the path through the B-cell as well as the location of the free energy barrier remains roughly the same. However, at the highest load of 56 bz/uc the β site local minima appear in the 2D maps,

and the free energy barrier is shifted towards the A-cell. Nevertheless, the overall diffusion path is still similar to the case at lower load.

The major conclusion of this analysis is that the diffusion path is approximately parallel to one of the coordinate axes (x or y), until an area of lower ΔG is reached in the B-cell. Then, the symmetrical path is followed along the other coordinate axis to the next A-cell. This overall picture remains valid for all investigated loadings. Thus, in order to gain a more quantitative insight into the free energy along the diffusion path, the spatial probability $q(r)$ for just a quarter of the unit cell (one A- and B-cell) has been integrated up orthogonal to the axis connecting the cells as shown in the insert in Fig. 6. The corresponding 1D free energy curves for the different loadings are shown in Fig. 6. Because of the integration over additional degrees of freedom, the ΔG values cannot be compared between the 3D, 2D and 1D cases. In particular, the 3D free energy map does not contain any translational contributions, whereas the 1D free energy profiles contains also the translational entropy perpendicular to the diffusion path. Again, the reduction of the free energy of the B-cell with respect to the A-cell for an increasing load is clearly visible. As a consequence, the free energy barrier at a value of $r^{\ddagger}$ around 15 Å is reduced from about 11 kJ/mol to about 8 kJ/mol going from 10 to 32 bz/uc. Detailed values, including the statistical errors, of the free energy barrier along this 1D diffusion pathways are given in Table 1. As already seen in the 2D plots, the free energy barrier is moved towards the A-cell ($r^{\ddagger}$ = 12 Å) for the highest load, because of the formation of the β site local minimum, visible as a small depression around r = 14 Å in the 1D curve. Thus, the free energy barrier $\Delta G^{\ddagger}$ is reduced by nearly a factor of two when going from 10 to 56 bz/uc. This also confirms the picture of a substantial guest–guest interaction, facilitating diffusion at intermediate loading, despite that fact that this is not clearly visible from the load dependence of D_{self} (Fig. 2).

From the pure transition state theory one would expect a substantial increase in the hopping rate from the A- to B-cell and thus the self-diffusion coefficient. However, as already investigated in great detail for the diffusion in other porous media like zeolites, a dynamical correction needs to be included to calculate the effective hopping rates. In other words, because of the guest–guest interactions, a strong stabilization of benzene molecules in the B-cell at higher load reduces the free energy barrier of the diffusion process. However, because of the fact that at high load most of the product sites are populated, more trajectories will recross, leading to a reduced effective rate over the transition state [82].

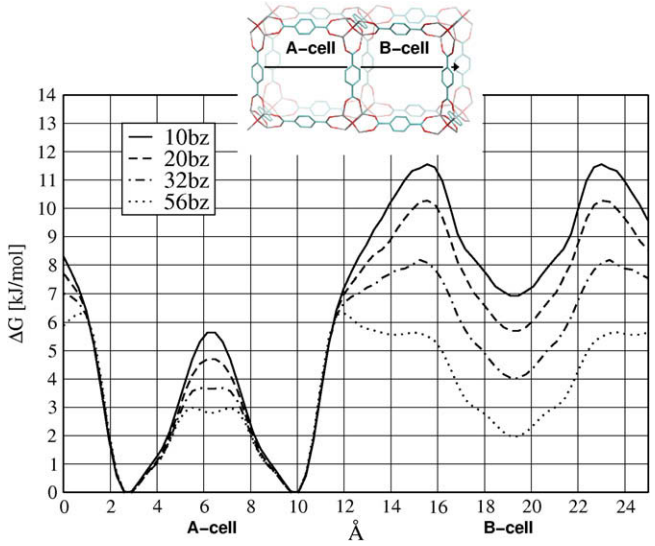

Fig. 6. Free Energy curve along the diffusion path of a benzene molecule along the axis connecting an A-cell (left) and a B-cell (right). The insert shows the part of the MOF-5 unit cell over which the integration has been performed, and the direction of the 1D diffusion path.

4. Conclusion

In this contribution, the diffusion mechanism of benzene guest molecules in the metal organic framework MOF-5 has been investigated by molecular dynamics simulations. We used a similar computational setup as in a previous work [48], and employed our fully flexible MM3 force field for MOF-5 [40]. In particular, the loading dependence was investigated by increasing the number of benzene molecules per unit cell from 10 to 20, 32 and 56. In all cases, the self-diffusion coefficients D_{self} are with values above 2×10^{-9} m^2/s in the range of liquid benzene, which demonstrates the open pore structure and high mobility of the guest molecules. A slight increase in D_{self} is found for intermediate loading, with the usual drop at higher load. From the 3D free energy maps certain sites, where the guest molecules localize, can be identified. The eight α_1 sites in the corners of the A-cell are populated first. Then the α_2 site in the center of the A-cell, and finally also the six β sites above the face of the B-cell are filled with increasing load. Because of the attractive guest–guest interactions the relative free energies of these sites change strongly with the loading. The distances between these sites, and also to the framework's phenylene units, correspond quite well to the radius of the first solvation shell in liquid benzene. Thus, the high guest mobility and the local structure confirm the view of MOF-5 as a "solid solvent". For all loads the diffusion mechanism consists of a motion from the global free energy minimum in the A-cell (α_1 site) through the adjacent B-cell into the next A-cell. The free energy barrier is reduced from 11.5 kJ/mol for 10 bz/uc to 6.3 kJ/mol for 56 bz/uc because of the stabilization by guest–guest interactions in the B-cell. Because of dynamical correction effects the effective hopping rate (and thus D_{self}) is, however, smaller than the rate resulting from transition state theory for these free energy barriers. Summarizing, one can say that MOF-5 represents a very open pore structure with liquid like mobilities for benzene. The diffusion process is not dominated by steric strain effects (when passing through a narrow pore window), but by specific attractive host–guest interactions leading to defined interaction sites within the framework. The diffusivity is, therefore, determined by the free energy that is necessary to leave these sites.

We have recently developed a new automated force field parametrization strategy [83], and are currently extending our force field in order to investigate the host guest interactions of other MOFs with the same methodology.

Acknowledgments

We would like to thank the Alfried Krupp von Halbach und Bohlen-Stiftung and the Deutsche Forschungsgemeinschaft (DFG SPP-1362) for financial support of this project. S.A. is grateful to the Fonds der Chemischen Industrie for a research stipend and to the Ruhr-University Research School for further financial support. In addition we would like to thank Randall Snurr, David Dubbledam and Frank Stallmach for helpful discussions.

References

[1] G. Ferey, Chem. Soc. Rev. 37 (2008) 191.
[2] S. Kitagawa, R. Kitaura, S. Noro, Angew. Chem. Int. Ed. 43 (2004) 2334.
[3] J.L.C. Rowsell, O.M. Yaghi, Micropor. Mesopor. Mater. 73 (2004) 3.
[4] U. Mueller, M. Schubert, F. Teich, H. Puetter, K. Schierle-Arndt, J. Pastre, J. Mater. Chem. 16 (2006) 626.
[5] M. Eddaoudi, J. Kim, N. Rosi, D. Vodak, J. Wachter, M. O'Keeffe, O.M. Yaghi, Science 295 (2002) 469.

[6] N. Rosi, J. Eckert, M. Eddaoudi, D. Vodak, H. Kim, M. O'Keeffe, O. Yaghi, Science 300 (2003) 1127.
[7] J.L.C. Rowsell, J. Eckert, O.M. Yaghi, J. Am. Chem. Soc. 127 (2005) 14904.
[8] Q.Y. Yang, C.L. Zhong, J. Phys. Chem. B 109 (2005) 11862.
[9] Q.Y. Yang, C.L. Zhong, J. Phys. Chem. B 110 (2006) 655.
[10] T. Yildirim, M.R. Hartman, Phys. Rev. Lett. 95 (2005) 215504.
[11] A. Samanta, T. Furuta, J. Li, J. Chem. Phys. 125 (2006) 084714.
[12] T. Sagara, J. Ortony, E. Ganz, J. Chem. Phys. 123 (2005) 214707.
[13] T. Sagara, J. Klassen, J. Ortony, E. Ganz, J. Chem. Phys. 123 (2005) 014701.
[14] T. Sagara, J. Klassen, E. Ganz, J. Chem. Phys. 121 (2004) 12543.
[15] F.M. Mulder, T.J. Dingemans, M. Wagemaker, G.J. Kearley, Chem. Phys. 317 (2005) 113.
[16] T. Mueller, G. Ceder, J. Phys. Chem. B 109 (2005) 17974.
[17] T.B. Lee, D. Kim, D.H. Jung, S.B. Choi, J.H. Yoon, J. Kim, K. Choi, S.H. Choi, Catal. Today 120 (2007) 330.
[18] E. Klontzas, A. Mavrandonakis, G.E. Froudakis, Y. Carissan, W. Klopper, J. Phys. Chem. C 111 (2007) 13635.
[19] D.H. Jung, D. Kim, T.B. Lee, S.B. Choi, J.H. Yoon, J. Kim, K. Choi, S.H. Choi, J. Phys. Chem. B 110 (2006) 22987.
[20] J.L.C. Rowsell, O.M. Yaghi, J. Am. Chem. Soc 128 (2006) 1304.
[21] J.L.C. Rowsell, A.R. Millward, K.S. Park, O.M. Yaghi, J. Am. Chem. Soc 126 (2004) 5666.
[22] S.S. Han, W.A. Goddard, J. Am. Chem. Soc. 129 (2007) 8422.
[23] H. Frost, T. Duren, R.Q. Snurr, J. Phys. Chem. B 110 (2006) 9565.
[24] G. Ferey, M. Latroche, C. Serre, F. Millange, T. Loiseau, A. Percheron-Guegan, Chem. Commun. (2003) 2976.
[25] D. Dubbeldam, H. Frost, K.S. Walton, R.Q. Snurr, Fluid Phase Equilibria 261 (2007) 152.
[26] C. Buda, B.D. Dunietz, J. Phys. Chem. B 110 (2006) 10479.
[27] A. Blomqvist, C.M. Araujo, P. Srepusharawoot, R. Ahuja, Proc. Natl. Acad. Sci. USA 104 (2007) 20173.
[28] A.W.C. van den Berg, S.T. Bromley, N. Ramsahye, T. Maschmeyer, J. Phys. Chem. B 108 (2004) 5088.
[29] E.J. Bautista, J.M. Seminario, Int. J. Quantum Chem. 108 (2008) 180.
[30] L. Sarkisov, T. Duren, R.Q. Snurr, Mol. Phys. 102 (2004) 211.
[31] A.I. Skoulidas, J. Am. Chem. Soc. 126 (2004) 1356.
[32] J. Kärger, D. Ruthven, Diffusion in Zeolites and Other Microporous Solids, Wiley & Sons, New York, 1992.
[33] B. Smit, T.L.M. Maesen, Chem. Rev. 108 (2008) 4125.
[34] F. Stallmach, S. Gröger, V. Künzel, J. Kärger, O.M. Yaghi, M. Hesse, U. Müller, Angew. Chem.-Int. Edit. 45 (2006) 2123.
[35] J.A. Greathouse, M.D. Allendorf, J. Phys. Chem. C 112 (2008) 5795.
[36] D. Dubbeldam, K.S. Walton, D.E. Ellis, R.Q. Snurr, Angew. Chem.-Int. Edit. 46 (2007) 4496.
[37] S.S. Han, W.A. Goddard, J. Phys. Chem. C 111 (2007) 15185.
[38] B.L. Huang, A.J.H. McGaughey, M. Kaviany, Int. J. Heat Mass Transfer 50 (2007) 393.
[39] N.A. Ramsahye, G. Maurin, S. Bourrelly, P.L. Llewellyn, T. Loiseau, C. Serre, G. Ferey, Chem. Commun. (2007) 3261.
[40] M. Tafipolsky, S. Amirjalayer, R. Schmid, J. Comput. Chem. 28 (2007) 1169.
[41] S. Keskin, J. Liu, R.B. Rankin, J.K. Johnson, D.S. Sholl, Ind. Eng. Chem. Res. 48 (2009) 2355.
[42] F. Salles, A. Ghoufi, G. Maurin, R.G. Bell, C. Mellot-Draznieks, G. Ferey, Angew. Chem.- Int. Edit. 47 (2008) 8487.
[43] H. Li, M. Eddaoudi, M. O'Keeffe, O.M. Yaghi, Nature 402 (1999) 276.
[44] S. Amirjalayer, R. Schmid, J. Phys. Chem. C 112 (2008) 14980.
[45] N.L. Allinger, Y.H. Yuh, J.-H. Lii, J. Am. Chem. Soc. 111 (1989) 8551.
[46] J.H. Lii, N.L. Allinger, J. Am. Chem. Soc. 111 (1989) 8566.
[47] J.H. Lii, N.L. Allinger, J. Am. Chem. Soc. 111 (1989) 8576.
[48] S. Amirjalayer, M. Tafipolsky, R. Schmid, Angew. Chem. Int. Ed. 46 (2007) 463.
[49] J. Kärger, H. Pfeifer, Magn. Res. Imag. 12 (1994) 235.
[50] J.L.C. Rowsell, E.C. Spencer, J. Eckert, J.A.K. Howard, O.M. Yaghi, Science 309 (2005) 1350.
[51] J.W. Ponder, F.M. Richards, J. Comput. Chem. 8 (1987) 1016. tinker version 4.2, June 2004, <http://dasher.wustl.edu/tinker/>.
[52] These distance cutoff values are standard values in MM3 force field calculations and have been used also in our previous investigations. Both long range interactions are tapered at the cutoff to avoid discontinuities. Note, that in MM3 bond dipole interactions are used instead of atomic point charges, which is the reason why a distance cutoff scheme can be used also for the electrostatic interactions.
[53] N.K. Allinger. <http://europa.chem.uga.edu/allinger/mm32000_new.html>.
[54] N.L. Allinger, F. Li, L. Yan, J.C. Tai, J. Comput. Chem. 11 (1990) 868.
[55] D. Beeman, J. Comput. Phys 20 (1976) 130.
[56] W. Hoover, Phys. Rev. A 31 (1985) 1695.
[57] S. Nose, Mol. Phys. 52 (1984) 255.
[58] Y.-C. Liu, Q. Wang, X.-F. Li, J. Chem. Phys. 122 (2005) 044714.
[59] Y.-C. Liu, Q. Wang, X.-F. Li, Chem. Phys. Lett. 432 (2006) 78.
[60] Y.-C. Liu, Q. Wang, X.-F. Li, J. Chem. Phys. 110 (1999) 11511.
[61] S.C. Harvey, K.-Z.R. Tan, T.E. Cheatham III, J. Comp. Chem 19 (1998) 726.
[62] W. Humphrey, A. Dalke, K. Schulten, J. Mol. Graphics 14 (1996) 33.
[63] N. Del Campo, M. Besnard, J. Yarwood, Chem. Phys. 142 (1990) 91.
[64] J. Kärger, H. Pfeifer, Zeolites 7 (1987) 90.
[65] D.R. Falcone, D.C. Douglass, D.W. McCall, J. Phys. Chem. 71 (1967) 2754.
[66] A.F. Collings, R. Mills, Trans. Faraday Soc. 66 (1970) 2761.
[67] M.A. McCool, A.F. Collings, L. Woolf, J. Chem. Soc. Faraday Trans. I 68 (1972) 1489.
[68] A. Maliniak, A. Laaksonen, J. Kowalewski, P. Stilbs, J. Chem. Phys. 89 (1988) 6434.
[69] P. Linse, S. Engström, B. Jönsson, Chem. Phys. Lett. 115 (1985) 95.
[70] R. Witt, S.L.A. Dölle, F. Müller-Plathe, J. Phys. Chem. A 104 (2000) 5716.
[71] M. Schwartz, D. Duan, R.J. Berry, J. Phys. Chem. A 109 (2005) 8637.
[72] T. Mosell, G. Schrimpf, J. Brickmann, J. Phys. Chem. B 101 (1997) 9485.
[73] H. Jobic, A.N. Fitch, J. Combet, J. Phys. Chem. B 104 (2000) 8491.
[74] D. Dubbeldam, E. Beerdsen, T.J.H. Vlugt, B. Smit, J. Chem. Phys. 122 (2005) 224712.
[75] M. Rubes, O. Bludsky, Phys. Chem. Chem. Phys. 10 (2008) 2611.
[76] M. Sinnokrot, E. Valeev, C. Sherrill, J. Am. Chem. Soc. 124 (2002) 10887.
[77] T. Tassaing, M.I. Cabaco, Y. Danten, M. Besnard, J. Chem. Phys. 113 (2000) 3758.
[78] M.I. Cabaco, Y. Danten, M. Besnard, Y. Guissani, B. Guillot, Chem. Phys. Let. 262 (1996) 120.
[79] J. Nagy, V.H. Smith, D.F. Weaver, J. Phys. Chem. 99 (1995) 13868.
[80] H. Kim, H. Chun, G.H. Kim, H.S. Lee, K. Kim, Chem. Commun. (2006) 2759.
[81] S. Hermes, F. Schröder, S. Amirjalayer, R. Schmid, R.A. Fischer, J. Mater. Chem. 16 (2006) 2464.
[82] Note, that another reason for the deviation between the hopping rates, determined from transition state theory and the effective hopping rates derived from D_{self} are due to the inappropriate choice of the reaction coordinate [74]. From the 2D free energy maps in Fig. 5 we see, however, that the diffusion path at the free energy maximum has a high projection on the chosen coordinate axis used for the 1D analysis (Fig. 6).
[83] M. Tafipolsky, R. Schmid, J. Phys. Chem. B 113 (2009) 1341.